Inorganic Chemistry

Article

pubs.acs.org/IC

Targeted Structure Modulation of "Pillar-Layered" Metal–Organic Frameworks for CO_2 Capture

Zhi-Hong Xuan, Da-Shuai Zhang, Ze Chang,* Tong-Liang Hu, and Xian-He Bu*

Department of Chemistry, Tianjin Key Lab on Metal and Molecule-based Material Chemistry, and Collaborative Innovation Center of Chemical Science and Engineering (Tianjin), Nankai University, Tianjin 300071, People's Republic of China

Supporting Information

ABSTRACT: Two new zinc MOFs with similar "pillar-layered" framework structures based on 1,1′-biphenyl-2,2′,6,6′-tetracarboxylic acid (H_4bpta) and two different bipyridine pillar ligands, namely $\{[Zn_4(bpta)_2(4\text{-pna})_2(H_2O)_2]\cdot 4DMF\cdot 3H_2O\}_n$ (**1**) and $\{[Zn_2(bpta)(bpy\text{-ea})(H_2O)]\cdot 2DMF\cdot H_2O\}_n$ (**2**) (4-pna = *N*-(4-pyridyl)-isonicotinamide and bpy-ea = 1,2-bis(4-pyridyl)ethane), have been synthesized and investigated with their CO_2 adsorption properties. By analysis of the structure properties and the CO_2 adsorption performances of these two MOFs, it was found that the introduction of polar acylamide groups via 4-pna resulted in **1** with enhanced CO_2 capacity and CO_2/CH_4 selectivity at low pressure. In contrast, the framework of **2** shows flexible properties originating from the flexibility of the ethanediylidene group in the bpy-ea ligand, which benefits the sieve effect of pores to give higher CO_2/CH_4 selectivity at a relatively high pressure range.

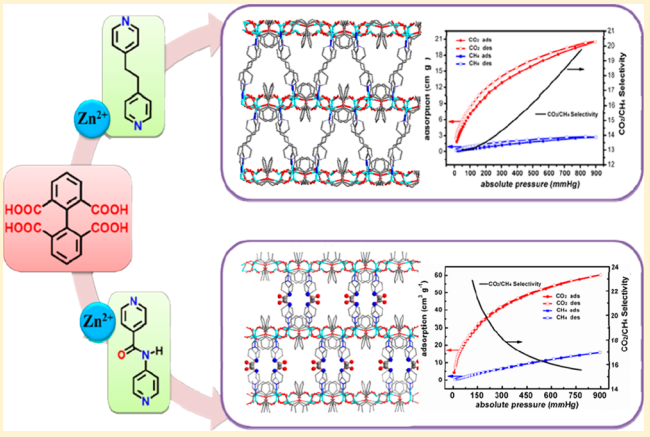

INTRODUCTION

The burning of fossil fuels leads to serious problems of the greenhouse effect, making carbon dioxide capture and storage one of the hottest topics in the chemistry domain.[1] Recently, using porous materials for CO_2 storage has been proved to be an efficient and promising method.[2] Metal–organic frameworks (MOFs), as one of the candidates for CO_2-absorbent materials, have received great attention because of their permanent porosity, high surface area, large pore volume, and adjustable pore size and shape.[3] Though the structure characteristics of MOFs can be tuned easily, it is still a challenge to construct MOFs with desired sorption and separation properties, since their performances are determined by many factors.[4] Recent research by our group and others indicate that the "pillar-layer" method is an effective strategy to synthesis porous MOFs. For example, we have reported a series of "pillar-layered" zinc MOFs based on 1,1′-biphenyl-2,2′,6,6′-tetracarboxylic acid (H_4bpta), which show robust frameworks with adjustable pore volume and window size depending on the length of bipyridine pillar ligands.[5] Also, in this system, functional groups could be introduced into the pore surface via the pillar ligand to modulate the pore surface toward the desired properties. Owing to the enhanced interactions between the acylamide groups and CO_2 molecules,[6] it has been reported that MOFs with acylamide-functionalized pore surfaces could show excellent performance in CO_2 storage; on the other hand, it is well-known that the sorption selectivity of MOFs could also be determined by the sieve effect of the aperture of the pore, which may result in high selectivity.[7]

With our continuous effort toward the design and synthesis of functional porous MOFs for CO_2 storage, we have tried to introduce functionalized pillar ligands into the "pillar-layered" zinc MOFs to get materials with improved performances. Herein, we report two "pillar-layered" MOFs with *N*-(4-pyridyl)isonicotinamide (4-pna) and 1,2-bis(4-pyridyl)ethane (bpy-ea) as pillar ligands, respectively, namely $\{[Zn_4(bpta)_2(4\text{-pna})_2(H_2O)_2]\cdot 4DMF\cdot 3H_2O\}_n$ (**1**) and $\{[Zn_2(bpta)(bpy\text{-ea})(H_2O)]\cdot 2DMF\cdot H_2O\}_n$ (**2**). Both MOFs show similar framework structures with different pore surfaces and flexibilities, which results in distinct CO_2 and CH_4 adsorption properties. By analysis of the structure properties and the CO_2 adsorption performances of these two MOFs, it was found that the introduction of polar acylamide groups via 4-pna resulted in **1** with enhanced CO_2 capacity and CO_2/CH_4 selectivity at low pressure. In contrast, the framework of **2** shows flexible properties originating from the flexibility of the ethanediylidene group in bpy-ea ligand, which benefits the sieve effect of pores to give higher CO_2/CH_4 selectivity at a relatively high pressure range.

Received: April 17, 2014
Published: August 15, 2014

   dx.doi.org/10.1021/ic500905z | *Inorg. Chem.* 2014, 53, 8985–8990

EXPERIMENTAL SECTION

Materials and Physical Measurements. Unless they were specialized, all solvents and reagents were obtained commercially and used as received. H_4bpta[8] and 4-pna[9] were synthesized according to the reported methods. IR spectra were measured on a TENSOR 27 OPUS (Bruker) FT-IR spectrometer using KBr disks dispersed with sample powders in the 4000−400 cm^{-1} range. Elemental analyses (C, H, and N) were performed on a PerkinElmer 240C analyzer. Thermogravimetric analyses (TGA) were carried out on a Rigaku standard TG-DTA analyzer with a heating rate of 10 °C min^{-1} from ambient temperature to 800 °C; an empty Al_2O_3 crucible was used as the reference. The room-temperature X-ray powder diffraction spectra (XRPD) were recorded on a Rigaku D/Max-2500 diffractometer at 40 kV and 100 mA with a Cu-target tube and a graphite monochromator. The temperature-dependent X-ray powder diffraction patterns were recorded with a Bruker D8 diffractometer at 40 kV and 40 mA with a Cu-target tube and a graphite monochromator. Simulation of the XRPD patterns was carried out by the single-crystal data and diffraction-crystal module of the Mercury (Hg) program, available free of charge via the Internet at http://www.iucr.org.

Syntheses. Single crystals of complexes **1** and **2** suitable for X-ray analysis were obtained by similar methods; thus, only the synthesis of **1** is described in detail.

*{[Zn_4(bpta)$_2$(4-pna)$_2$(H_2O)$_2$]·4DMF·3H_2O}$_n$ (**1**).* $Zn(NO_3)_2·6H_2O$ (0.1 mmol), 4-pna (0.05 mmol) and H_4bpta (0.05 mmol) were added to a DMF/ethanol/H_2O mixture (v/v/v 4:1:2, 14 mL), sealed in a capped vial and ultrasonicated to give a clear solution. Then the vial was capped and kept at 85 °C for 24 h. The homogeneous colorless crystals that formed were collected by filtration, washed with DMF, and dried in air (yield 60% based on H_4bpta). FT-IR (KBr pellets, cm^{-1}): 3403 m, 3066 w, 2931 w, 1663 s, 1603 s, 1577 s, 1557 s, 1460 m, 1432 m, 1385 s, 1339 m, 1100 w, 834 m, 777 m, 709 m, 538 w, 448 w. Anal. Calcd for $C_{66}H_{68}N_{10}O_{27}Zn_4$: C, 46.77; H, 4.04; N, 8.26. Found: C, 46.65; H, 4.37; N, 8.01.

*{[Zn_2(bpta)(bpy-ea)(H_2O)]·2DMF·H_2O}$_n$ (**2**).* This compound was synthesized by a procedure similar to that for **1**, with 4-pna replaced by bpy-ea. FT-IR (KBr pellets, cm^{-1}): 3422 m, 3076 w, 2934 w, 1669 s, 1605 s, 1576 s, 1553 s, 1459 m, 1436 m, 1383 s, 1276 m, 1070 w, 833 m, 777 m, 717 m, 539 w, 447 w. Anal. Calcd for $C_{34}H_{18}N_4O_{12}Zn_2$: C, 50.7; H, 2.25; N, 6.95. Found: C, 50.4; H, 2.53; N, 7.25.

X-ray Data Collection and Structure Determinations. Single-crystal X-ray diffraction measurements for **1** and **2** were carried out on a Rigaku Saturn724+ diffractometer at 113 K. The determinations of unit cell parameters and data collections were performed with Mo Kα radiation (λ = 0.71073 Å), and unit cell dimensions were obtained with least-squares refinements. The program SAINT[10] was used for integration of the diffraction profiles. Semiempirical absorption corrections were applied using the SADABS program. The structure was solved by direct methods using the SHELXS program of the SHELXTL package and refined with SHELXL.[11] Zinc atoms were found from *E* maps, and other non-hydrogen atoms were located in successive difference Fourier syntheses. The final refinement was performed by full-matrix least-squares methods with anisotropic thermal parameters for non-hydrogen atoms on F^2. The hydrogen atoms were added theoretically, riding on the concerned atoms, and refined with fixed thermal factors except for H_2O molecules. The solvent DMF molecules in **2** were disordered. In addition, the disorder was treated by performing split occupancy refinement of the disordered atoms. Crystallographic data and refinement parameters are given in Table 1. The selected bond lengths and angles are given in Table S1 (Supporting Information).

Sorption Measurements. Gas adsorption measurements were performed using an ASAP 2020 M gas adsorption analyzer. UHP-grade gases were used in the measurements. The N_2 isotherm measurements were carried out at 77, 273, and 298 K, and the CO_2 and CH_4 sorption isotherms were collected at 273 and 298 K, respectively, for the two complexes.

Before measurements, the samples were soaked in methanol for 3 days to exchange DMF and H_2O solvent and then filtered and dried at room temperature. The dried samples were loaded in sample tubes and activated under high vacuum (less than 10^{-5} Torr) at 150 °C. About 100 mg of degassed samples was used for gas sorption measurements, and the weight of each sample was recorded before and after outgassing to confirm the removal of guest molecules. The outgassing procedure was repeated on the same sample between experiments for 0.5−1 h.

Table 1. Crystal Data and Structure Refinement Parameters for Complexes 1 and 2

	1	2
empirical formula	$C_{66}H_{68}N_{10}O_{27}Zn_4$	$C_{34}H_{36}N_4O_{12}Zn_2$
formula wt	1694.78	823.41
temp/K	113	113
cryst syst	monoclinic	monoclinic
space group	*C*2/*c*	$P2_1/c$
a/Å	30.186(6)	13.801(3)
b/Å	13.928(2)	13.687(3)
c/Å	18.957(4)	19.144(4)
β/deg	114.668(3)	102.84(3)
V/Å^3	7243(2)	3525.8(13)
Z	4	4
D_c/g cm^{-3}	1.554	1.551
F(000)	3480	1696
θ range/deg	2.20−27.87	1.65−20.05
no. of rflns collected	36208	29938
no. of indep rflns	8598	7772
goodness of fit	1.096	1.04
R1[a] ($I > 2\sigma(I)$)	0.0687	0.0777
wR2[b] ($I > 2\sigma(I)$)	0.1653	0.2263

[a] $R1 = \sum||F_o| - |F_c||/\sum|F_o|$. [b] $wR2 = [\sum[w(F_o^2 - F_c^2)^2]/\sum(F_o^2)^2]]^{1/2}$.

RESULTS AND DISCUSSION

Synthesis. As we reported before, solvothermal reactions of $Zn(NO_3)_2·6H_2O$ with H_4bpta tends to form [Zn_4(bpta)$_2$(H_2O)$_2$] layer structure.[5] Utilizing this characteristic, 4-pna and bpy-ea were introduced to produce "pillar-layered" MOFs **1** and **2**, with acylamide- and alkyl-functionalized pore surfaces, respectively. The framework structure of **1** is just the same as that we reported before, while the framework of **2** shows a different arrangement of pillar ligands. It should be noted that, though the framework of **2** is slightly different from that of **1**, the layer structures as well as the accessible volumes of the framework are nearly the same, indicating the stability of the assembled system.

Crystal Structure of {[Zn_4(bpta)$_2$(4-pna)$_2$(H_2O)$_2$]·4DMF·3H_2O}$_n$ (1). Crystallographic analysis reveals that **1** crystallizes in the monoclinic *C*2/*c* space group. As shown in Figure 1a, the asymmetric unit of **1** contains two crystallographically independent Zn(II) centers, one bpta^{4-} ligand and one 4-pna ligand. The Zn1 center is six-coordinated to four oxygen atoms from three carboxylate groups of two bpta^{4-} ligands, one N atom from 4-pna, and one H_2O molecule (Zn−O, 2.02−2.20 Å; Zn−N, 2.09 Å). The Zn2 ion is four-coordinated by three carboxylate O atoms from three different bpta^{4-} ligands and one N atom from the 4-pna ligand (Zn−O, 1.93−1.96 Å; Zn−N, 2.01 Å), which results in a tetrahedral geometry. One of the carboxylate groups coordinates to the metal center with a chelating mode and the other two with a monodentate mode. Each bpta^{4-} ligand coordinates with five Zn(II) centers, which results in a complicated two-dimensional (2D) layer (Figure 1b). A three-dimensional (3D) "pillar-layered" structure (Figures 1c,d) is generated when the adjacent layers are

dx.doi.org/10.1021/ic500905z | Inorg. Chem. 2014, 53, 8985−8990

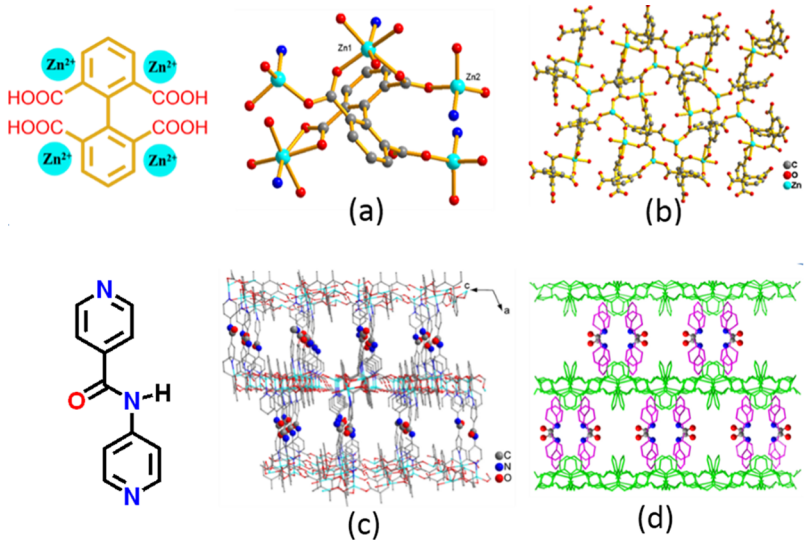

Figure 1. Crystal structure of **1**: (a) coordination environment of Zn(II) ions and $bpta^{4-}$; (b) views of the 2D layer assembled by Zn(II) ions and $bpta^{4-}$ ligands; (c) views in parallel with the channels along the *b* direction; (d) views in parallel with the channels along the *c* direction.

connected through 4-pna ligands coordinated to Zn(II) centers. The space between the layers is occupied by solvent DMF and H_2O molecules. After removal of solvent molecules filled in the pore space, the accessible volume is 36.6%, as estimated using the SOLV function of PLATON.[12]

The network contains channels running along the *b* and *c* axes. For the channel along the *b* axis, the opening has a size of ~4.9 × 3.7 $Å^2$ (*a* × *c*) (Figure 1d) and along the *c* axis the dimension is ~3.5 × 3.2 $Å^2$ (*a* × *b*) (Figure 1c), excluding the van der Waals radius of atoms. As shown in Figure 1c,d, the 4-pna ligands pillared the layers to give the channels, and the channel wall was functionalized by the acylamide groups in 4-pna ligands. It should be noted that, though the acylamide linker in this compound is larger than the azo linker we reported before, the aperture size along the *b* axis did not show significant changes, while the aperture size in the *c* direction has been reduced. This should be attributed to the orientation of the flexible acylamide linker.

Crystal Structure of $\{[Zn_2(bpta)(bpy\text{-}ea)(H_2O)]\cdot 2DMF\cdot H_2O\}_n$ (2). Complex **2** crystallizes in $P2_1/c$ space group. The layers in complex **2** has the same connection mode as that in **1**, while the bond distances and angles are slightly changed (see the Supporting Information for details). The network of complex **2** also contains channels running along the *b* and *c* axes. For the channel along the *b* axis, the opening has a size of ~3.2 × 3.6 $Å^2$ (*a* × *c*) and along the *c* axis the triangle dimension is ~3.2 × 3.2 × 2.7 $Å^3$, excluding the van der Waals radii of atoms. However, there are subtle differences in the arrangement of pillars in complex **2** in comparison with that of **1**. In complex **1**, the pillars are almost perpendicular to the layers both along *b* and *c* axes, while the adjacent bpy-ea ligands between the layers of **2** slightly sloped to the opposite direction along *c* axis, leading to the formation of triangle channels (Figure 2b), which is different from the almost squared channels in **1**. This should be attributed to the staggering of the layers along the *b* direction, which affects the connection of pillar ligands. After removal of solvent molecules filled in the pore space, the accessible volume is 36.9%, as estimated using the SOLV function of PLATON.[12] Similar to that of **1**, the channel wall was defined by the ethanediylidene group of bpy-ea ligands.

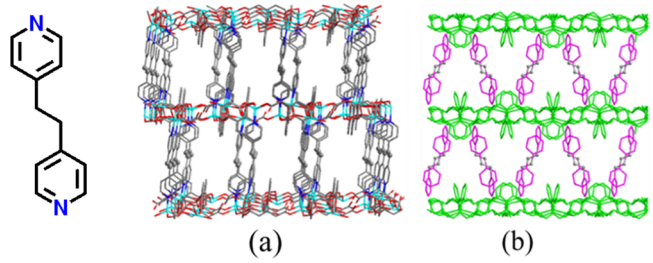

Figure 2. Crystal structure of **2**: (a) views in parallel with the channels along the *b* direction; (b) views in parallel with the channels along the *c* direction.

X-ray Powder Diffraction. Powder X-ray diffraction (PXRD) was conducted to confirm the phase purity of complexes **1** and **2** as well as their stability upon solvent exchange. The good match of patterns of the as-synthesized samples with the simulated patterns from the single-crystal structures suggests the high phase purity of complexes **1** and **2** (Figures S1 and S2, Supporting Information). Furthermore, the patterns of the methanol-exchanged samples reveal that the solvent-exchanged samples are still crystalline.

It should be noted that a new peak emerged around the first main peak at 6.4° after the solvent exchange for **2**, and the peak disappeared after the activation process. According to the crystal structure, the first main peak should be assigned to the layer structure in the framework (indexed as (2,0,0)); then the new peak observed at high angle area just indicates a structural periodicity with shorter interdistance. Interestingly, no similar phenomenon has been observed in the MOFs with rigid pillar ligands. Then this phenomenon should be attributed to the flexibility of the bpy-ea ligand: the flexible pillar ligand could undergo a conformation orientation to shorten the interlayer distance upon the exchange of guest solvent molecules (DMF to methanol), and the conformation is restored when the guest molecules are removed in the activation process.

On the other hand, though the 4-pna ligand in **1** is also flexible, there was no obvious change of the pattern after the solvent exchange. This might be attributed to the N−H···O interactions between the DMF molecules and the acylamide groups in 4-pna ligands, which anchored the guests. This

dx.doi.org/10.1021/ic500905z | Inorg. Chem. 2014, 53, 8985−8990

speculation is further proved by the TGA results of complex **1**. This result suggests that guest-dependent structure response of the pillar-layered MOFs might be achieved by introducing flexible pillar ligands.

In order to further verify the thermal stability of complexes **1** and **2**, we have carried out the temperature-dependent X-ray powder diffraction measurements (Figures S3 and S4, Supporting Information), and the data analysis showed that the two porous MOFs have good thermal stability. However, there are some shifts and disappearance of several peaks as well as the appearance of a few new peaks, which might be attributed to the flexibility of the framework and the distortion of the crystal lattice in response to the removal of guest molecules.[5] In addition, we tested the reversibility of the phrase change of the MOFs by PXRD. When the activated samples were soaked into DMF again, their PXRD patterns showed that some peaks which disappeared or shifted during the active process have appeared again or moved back to almost their original positions (Figures S1 and S2, Supporting Information), which further confirmed the flexibility of the framework.

Thermogravimetric Analyses. To examine the thermal stability of the obtained MOFs, thermogravimetric analyses (TGA) experiments were carried out (Figures S5 and S6, Supporting Information). As shown in the crystal structure analysis, complex **1** includes four DMF and three H_2O molecules as guests. The observed weight loss of the guest molecules (20.4%) is in agreement with that calculated for the corresponding crystal structure (21%). After the sample was soaked in methanol for 3 days, the TG curve did not show obvious change, which indicated that the solvent molecules are not exchanged. This might be due to the relatively strong hydrogen bond between the guest DMF and the pillar ligand as we discussed above. On the other hand, there was no weight loss until 380 °C for the activated sample, showing the successful removal of the solvent molecules during the activation process.

The TG curve of complex **2** showed no weight loss before 100 °C, and then it reveals a weight loss of 13.7% in the temperature range 100−219 °C. After solvent exchange with methanol, the TG curve showed a weight loss of 8% in the temperature range 36−92 °C, which could be attributed to the loss of solvent molecules residing in the open channels. Also, the activated sample **2** shows high thermal stability up to 380 °C, indicating the high thermal stability of these pillar-layered MOFs.

Porosity Characterization. Nitrogen gas adsorption experiments at 77 K were explored for the pore characterization of complexes **1** and **2** (Figure 3). Before the measurement, all of the samples were activated at 150 °C to remove the guest solvent molecules. As shown in Figure 3, N_2 sorption isotherms of complex **1** present a type I kind behavior, indicating the microporosity of the complex. However, for complex **2**, the N_2 uptake is relatively low. These sorption curves were analyzed using the Brunauer−Emmett−Teller (BET) and Langmuir methods. The estimated apparent BET and Langmuir surface areas are 413 and 547 $m^2\ g^{-1}$ for **1** and 51 and 69 $m^2\ g^{-1}$ for **2**. Although the accessible volumes of the two complexes are similar (36.6% for **1** and 36.9% for **2**) on the basis of the crystal structure data, the N_2 adsorption results of these two compounds show distinct pore volumes (0.21 $cm^3\ g^{-1}$ for **1** and 0.03 $cm^3\ g^{-1}$ for **2**), less than the pore volumes estimated from the single-crystal structure (about 0.29 $cm^3\ g^{-1}$ for both **1** and **2**), which indicates the flexibility of the two complexes.

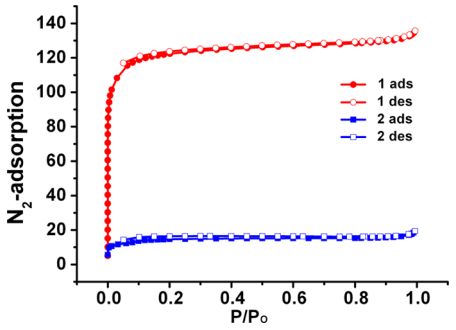

Figure 3. Isothermal adsorption curves of N_2 gas for **1** and **2** (activation was performed at 150 °C).

The surface area and pore volume of complex **1** is comparable to that of the MOFs with 4,4′-azopyridine as pillar ligand, since they have similar structures.[5] However, complex **2** showed significently decreased surface area and pore volume. This should be attributed to the decreased aperture size of the channels as well as the flexible nature of the framework of complex **2**, which may limit the entrance of N_2 molecules. It is supported by the fact that a relatively long time is required for the sorption equilibration to be achieved, indicating the low difussion rate of N_2 in the channel of complex **2** (Table S2, Supporting Information). On the basis of previous research, the relatively high porsity of **1** and the acylamide group introduced may result in better CO_2 adsorption capacity in comparison with that of **2**, while the limited pore size may benefit the CO_2 selectivity toward other molecules with larger dimensions.

CO_2 Adsorption Investigation. In order to investigate the CO_2 capture ability of complexes **1** and **2**, CO_2 adsorption isotherms were measured at 273 and 298 K for these complexes, respectively (Figures 4 and 5 and Figure S7 (Supporting Information)). For **1**, the maximum CO_2 capacity of adsorption is 60.31 $cm^{-3}\ g^{-1}$ at 273 K/900 mmHg and 41.95 $cm^{-3}\ g^{-1}$ at 298 K/900 mmHg, which are considerable in

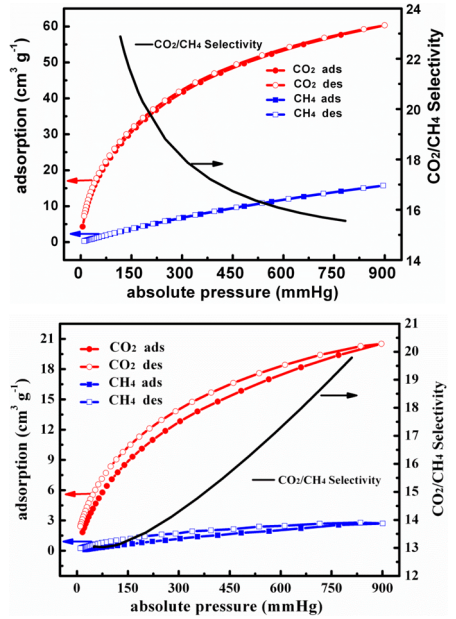

Figure 4. CO_2 and CH_4 adsorption capacity and the selectivity for carbon dioxide from an equimolar mixture of methane and carbon dioxide of complexes **1** (top) and **2** (bottom) at 273 K.

dx.doi.org/10.1021/ic500905z | Inorg. Chem. 2014, 53, 8985−8990

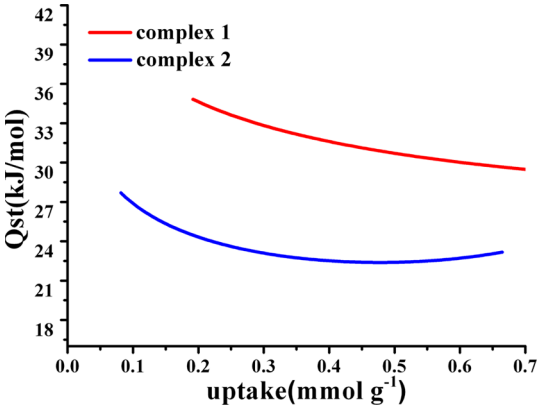

Figure 5. CO_2 adsorption enthalpies (Q_{st}) of complexes **1** and **2**.

comparison with its medium surface area. In comparison, the uptake of complex **2** is only 20.51 cm^{-3} g^{-1} at 273 K/900 mmHg and 14.89 cm^{-3} g^{-1} at 298 K/900 mmHg. It should be noted that, though complex **2** has a low CO_2 capacity of adsorption at 273 and 298 K, the maximum adsorption amounts are quite similar to those of N_2 at 77 K. Since the saturated N_2 adsorption amount achieved at $P/P^0 \approx 1$ defined the accessible pore volume at 77 K, the unsaturated CO_2 uptake indicates increased accessible space at 273 K. This attests to the flexible nature of the framework of complex **2**.

To evaluate the interaction between the adsorbed CO_2 molecules and the host framework, the CO_2 adsorption enthalpies (Q_{st}) of complexes **1** and **2** were calculated using the modified Clausius–Clapeyron equation by fitting adsorption isotherms at 273 K and 298 k (Figure 5 and Figures S10 and S11 (Supporting Information)).[13] The Q_{st} value of **1** for CO_2 is 34.82 kJ mol^{-1} at zero loading, reflecting a relatively strong CO_2–framework interaction, while for complex **2** the Q_{st} value is 27.69 kJ mol^{-1}. The relatively high Q_{st} value of **1** can be attributed to the enhanced interaction between CO_2 molecules and the polar acylamide groups, which could benefit the capture and selective adsorption of CO_2.

To further investigate the CO_2 selectivity of these complexes, their CH_4 adsorption capacities were also tested at 273 K and the data were used to calculated the CO_2/CH_4 selectivity using the ideal adsorbed solution theory (IAST)[14] method (Figures 4 and 5). As shown in Figures 4 and 5, the selectivity of CO_2 over CH_4 for complex **1** reveals a decreasing trend from 23 to 15 in the range of 0–1 bar. These values are higher than those for some classical adsorbent MOFs, such as MOF-5,[15] Cu-BTC,[15] and NUJ-Bai3[6a] in the low-pressure range based on the IAST model and similar conditions, benefiting from the improved CO_2 storage capacities and enhanced CO_2 binding affinity of **1**.[16] More interesting, the CO_2/CH_4 selectivity of complex **2** shows an increasing trend from 13 to 19; this is quite rare in MOFs. In comparison with that of **1**, the selectivity of **2** is lower below 0.6 bar, and the value turns out to be higher beyond that point. Taking the structure of **2** into account, the increased selectivity should be attributed to the flexibility of its framework: as the pressure increases and gas molecules are adsorbed, a distortion of the framework may occur, which results in enhanced sieve effects and corresponding higher selectivity. The increased selectivity of **2** indicates that the enhanced sieve effect of the pores might be a key effect which could benefit CO_2 capture at relatively high pressure.

CONCLUSION

We have successfully constructed two new "pillar-layered" Zn MOFs which exhibit different CO_2 capture capacity and relatively high CO_2/CH_4 selectivity depending on the pillar ligands used. These results indicate that the introduction of acylamide groups in this pillar-layered MOF system could bring enhanced CO_2 uptake and CO_2/CH_4 selectivity at low pressure on the basis of an enhanced gas–framework interaction, while the utilization of a flexible ligand may contribute to the selectivity at higher pressure as a result of the enhanced sieve effect. These results indicate that the structure factors (pore dimension and flexibility) as well as the binding affinity could determine the CO_2 capture ability of MOFs. To construct MOFs with balanced CO_2 capacity and selectivity for CO_2 capture application, all of these factors should be considered. Then the results reported here may guide the design and synthesis of CO_2 capture targeted MOFs.

ASSOCIATED CONTENT

Supporting Information

CIF files giving X-ray crystallographic data for complexes **1** and **2**, Tables S1 and S2 and Figures S1–S11 (as described in the text), and text giving details of the analysis of gas sorption isotherms and prediction of the gas adsorption selectivity by IAST. This material is available free of charge via the Internet at http://pubs.acs.org.

AUTHOR INFORMATION

Corresponding Authors

*Z.C.: e-mail, changze@nankai.edu.cn; fax, +86-22-23502458.
*X.-H.B.: e-mail, buxh@nankai.edu.cn

Notes

The authors declare no competing financial interest.

ACKNOWLEDGMENTS

This work was financially supported by the 973 Program of China (2014CB845600), the NNSF of China (21031002, 21202088, and 21371102), and the MOE Innovation Team (IRT13022) of China.

REFERENCES

(1) (a) Duan, J. G.; Yang, Z.; Bai, J. F.; Zheng, B. S.; Li, Y. Z.; Li, S. H. *Chem. Commun.* **2012**, *48*, 3058. (b) Jacobson, M. Z. *Energ Environ. Sci.* **2009**, *2*, 148. (c) Li, J. R.; Kuppler, R. J.; Zhou, H. C. *Chem. Soc. Rev.* **2009**, *38*, 1477. (d) Li, J. R.; Sculley, J.; Zhou, H. C. *Chem. Rev.* **2012**, *112*, 869. (e) He, Y.-P.; Tan, Y.-X.; Zhang, J. *Inorg. Chem.* **2013**, *52*, 12758. (f) Li, J. R.; Lu, Y. W.; Sun, L. B.; Sculley, J.; Balbuena, P. B.; Zhou, H. C. *Nat. Commun.* **2013**, *4*, 1538. (g) Zhang, Z. J.; Yao, Z. Z.; Xiang, S. C.; Chen, B. L. *Energy Environ. Sci.* **2014**, DOI: 10.1039/c4ee00143e.

(2) (a) Rochelle, G. T. *Science* **2009**, *325*, 1652. (b) Arstad, B.; Blom, R.; Swang, O. *J. Phys. Chem. A* **2007**, *111*, 1222. (c) Burd, S. D.; Ma, S.; Perman, J. A.; Sikora, B. J.; Snurr, R. Q.; Thallapally, P. K.; Tian, J.; Wojtas, L.; Zaworotko, M. J. *J. Am. Chem. Soc.* **2012**, *134*, 3663. (d) Mohamed, M. H.; Elsaidi, S. K.; Wojtas, L.; Pham, T.; Forrest, K. A.; Tudor, B.; Space, B.; Zaworotko, M. J. *J. Am. Chem. Soc.* **2012**, *134*, 19556. (e) Nugent, P. S.; Rhodus, V. L.; Pham, T.; Forrest, K.; Wojtas, L.; Space, B.; Zaworotko, M. J. *J. Am. Chem. Soc.* **2013**, *135*, 10950. (f) Wang, J.; Luo, J.; Zhao, J.; Li, D. S.; Li, G.; Huo, Q.; Liu, Y. *Cryst. Growth Des.* **2014**, *14*, 2375.

(3) (a) Millward, A. R.; Yaghi, O. M. *J. Am. Chem. Soc.* **2005**, *127*, 17998. (b) Llewellyn, P. L.; Bourrelly, S.; Serre, C.; Vimont, A.; Daturi, M.; Hamon, L.; De Weireld, G.; Chang, J. S.; Hong, D. Y.; Hwang, Y. K.; Jhung, S. H.; Férey, G. *Langmuir* **2008**, *24*, 7245. (c) Awwad, A.

M.; Ai-Dujaili, A. H.; Essa, H. M. *J. Chem. Eng. Data* **2004**, *49*, 741. (d) Himeno, S.; Komatsu, T.; Fujita, S. *J. Chem. Eng. Data* **2005**, *50*, 369. (e) Zheng, B. S.; Yang, Z.; Bai, J. F.; Li, Y. H.; Li, S. H. *Chem. Commun.* **2012**, *48*, 7025. (f) Li, J. R.; Ma, Y. G.; McCarthy, M. C.; Sculley, J.; Yu, J. M.; Jeong, H. K.; Balbuena, P. B.; Zhou, H. C. *Coord. Chem. Rev.* **2011**, *255*, 1791. (g) Ma, S. Q.; Zhou, H. C. *Chem. Commun.* **2010**, *46*, 44. (h) Xiong, S.; He, Y.; Krishna, R.; Chen, B.; Wang, Z. *Cryst. Growth Des.* **2013**, *13*, 2670. (i) Chen, Z.; Xiang, S.; Arman, H. D.; Mondal, J. U.; Li, P.; Zhao, D.; Chen, B. *Inorg. Chem.* **2011**, *50*, 3442.

(4) (a) Yuan, D. Q.; Zhao, D.; Sun, D. F.; Zhou, H. C. *Angew. Chem., Int. Ed.* **2010**, *49*, 5357. (b) Babarao, R.; Jiang, J. W. *Langmuir.* **2008**, *24*, 6270. (c) Furukawa, H.; Ko, N.; Go, Y. B.; Aratani, N.; Choi, S. B.; Choi, E.; Yazaydin, A. O.; Snurr, R. Q.; O'Keeffe, M.; Kim, J.; Yaghi, O. M. *Science* **2010**, *329*, 424.

(5) Chang, Z.; Zhang, D. S.; Chen, Q.; Li, R. F.; Hu, T. L.; Bu, X. H. *Inorg. Chem.* **2011**, *50*, 7555.

(6) (a) Duan, J.; Yang, Z.; Bai, J.; Zheng, B.; Li, Y.; Li, S. *Chem. Commun.* **2012**, *48*, 3058. (b) Vaidhyanathan, R.; Iremonger, S. S.; Dawson, K. W.; Shimizu, G. K. H. *Chem. Commun.* **2009**, 5230. (c) Zheng, B.; Yang, Z.; Bai, J.; Li, Y.; Li, S. *Chem. Commun.* **2012**, *48*, 7025. (d) Zou, Y.; Park, M.; Hong, S.; Lah, M. S. *Chem. Commun.* **2008**, 2340. (e) Xiong, S.; He, Y.; Krishna, R.; Chen, B.; Wang, Z. *Cryst. Growth Des.* **2013**, *13*, 2670. (f) García-Ricard, O. J.; Silva-Martínez, J. C.; Hernández-Maldonado, A. J. *Dalton Trans.* **2012**, *41*, 8922. (g) Liu, B.; Li, D. S.; Hou, L.; Yang, G. P.; Wang, Y. Y.; Shi, Q. Z. *Dalton Trans.* **2013**, *42*, 9822. (h) Lee, C. H.; Huang, H. Y.; Liu, Y. H.; Luo, T. T.; Lee, G. H.; Peng, S. M.; Jiang, J. C.; Chao, I.; Lu, K. L. *Inorg. Chem.* **2013**, *52*, 3962. (i) Zheng, B.; Bai, J.; Duan, J.; Wojtas, L.; Zaworotko, M. J. *J. Am. Chem. Soc.* **2011**, *133*, 748. (j) Hasegawa, S.; Horike, S.; Matsuda, R.; Furukawa, S.; Mochizuki, K.; Kinoshita, Y.; Kitagawa, S. *J. Am. Chem. Soc.* **2007**, *129*, 2607. (h) Xiang, S.; He, Y.; Zhang, Z.; Wu, H.; Zhou, W.; Krishna, R.; Chen, B. *Nat. Commun.* **2012**, *3*, 954.

(7) (a) Hou, L.; Shi, W. J.; Wang, Y. Y.; Guo, Y.; Jin, C.; Shi, Q. Z. *Chem. Commun.* **2011**, *47*, 5464. (b) Choi, E. Y.; Park, K.; Yang, C.-M.; Kim, H.; Son, J. H.; Lee, S. W.; Lee, Y. H.; Min, D.; Kwon, Y. U. *Chem. Eur. J.* **2004**, *10*, 5535. (c) Henke, S.; Schmid, R.; Grunwaldt, J.-D.; Fischer, R. A. *Chem. Eur. J.* **2010**, *16*, 14296. (d) Li, J. R.; Tao, Y.; Yu, Q.; Bu, X. H.; Sakamoto, H.; Kitagawa, S. *Chem. Eur. J.* **2008**, *14*, 2771. (e) Chen, B.; Ma, S.; Zapata, F.; Fronczek, F. R.; Lobkovsky, E. B.; Zhou, H. C. *Inorg. Chem.* **2007**, *46*, 1233.

(8) Pryor, K. E.; Shipps, G. W.; Skyler, D. A.; Rebek, J. *Tetrahedron* **1998**, *54*, 4107.

(9) Qin, Z. Q.; Jennings, M. C.; Puddephatt, R. J. *Chem. Commun.* **2001**, 2676.

(10) *SAINT Software Reference Manual*; Bruker AXS: Madison, WI, 1998.

(11) Sheldrick, G. M. *SHELXTL NT, Version 5.1 (Program for Solution and Refinement of Crystal Structures)*; University of Göttingen, Göttingen, Germany, 1997. Spek, A. L. *J. Appl. Crystallogr.* **2003**, *36*, 7.

(12) Spek, A. L. *J. Appl. Crystallogr.* **2003**, *36*, 7.

(13) Zhong, D. C.; Lin, J. B.; Lu, W. G.; Jiang, L.; Lu, T. B. *Inorg. Chem.* **2009**, *48*, 8656.

(14) Bae, Y. S.; Mulfort, K. L.; Frost, H.; Ryan, P.; Punnathanam, S.; Broadbelt, L. J.; Hupp, J. T.; Snurr, R. Q. *Langmuir* **2008**, *24*, 8592.

(15) Yang, Q.; Zhong, C. *ChemPhysChem* **2006**, *7*, 1417.

(16) (a) Dietzel, P. D. C.; Besikiotis, V.; Blom, R. *J. Mater. Chem.* **2009**, *19*, 7362. (b) Caskey, S. R.; Wong-Foy, A. G.; Matzger, A. J. *J. Am. Chem. Soc.* **2008**, *130*, 10870. (c) Aprea, P.; Caputo, D.; Gargiulo, N.; Iucolano, F.; Pepe, F. *J. Chem. Eng. Data* **2010**, *55*, 3655. (d) Pachfule, P.; Chen, Y. F.; Jiang, J. W.; Banerjee, R. *J. Mater. Chem.* **2011**, *21*, 17737. (e) Panda, T.; Pachfule, P.; Chen, Y. F.; Jiang, J. W.; Banerjee, R. *Chem. Commun.* **2011**, *47*, 2011. (f) Furukawa, H.; Kim, J.; Ockwig, N. W.; O'Keeffe, M.; Yaghi, O. M. *J. Am. Chem. Soc.* **2008**, *130*, 11650. (g) Lin, Q. P.; Wu, T.; Zheng, S. T.; Bu, X. H.; Feng, P. Y. *J. Am. Chem. Soc.* **2012**, *134*, 784. (h) Banerjee, R.; Furukawa, H.; Britt, D.; Knobler, C.; O'Keeffe, M.; Yaghi, O. M. *J. Am. Chem. Soc.* **2009**, *131*, 3875. (i) Neofotistou, E.; Malliakas, C. D.; Trikalitis, P. N. *Chem. Eur. J.* **2009**, *15*, 4523. (j) Tian, Y. Q.; Yao, S. Y.; Gu, D.; Cui, K. H.; Guo, D. W.; Zhang, G.; Chen, Z. X.; Zhao, D. Y. *Chem. Eur. J.* **2010**, *16*, 1137. (k) Liu, X. M.; Lin, R. B.; Zhang, J. P.; Chen, X. M. *Inorg. Chem.* **2012**, *51*, 5686. (l) Mallick, A.; Kundu, T.; Banerjee, R. *Chem. Commun.* **2012**, *48*, 8829. (m) Chen, Z. X.; Xiang, S. C.; Arman, H. D.; Li, P.; Zhao, D. Y.; Chen, B. L. *Eur. J. Inorg. Chem.* **2011**, 2227. (n) An, J.; Geib, S. J.; Rosi, N. L. *J. Am. Chem. Soc.* **2010**, *132*, 38. (o) Wang, F.; Tan, Y. X.; Yang, H.; Kang, Y.; Zhang, J. *Chem. Commun.* **2012**, *48*, 4842.